ELSEVIER

May 1995

Pattern Recognition Letters 16 (1995) 517–529

Pattern Recognition Letters

# A pattern recognition approach to the detection of complex edges

Dov Dori [a,*], Robert M. Haralick [b]

[a] *Department of Information Systems Engineering, Faculty of Industrial Engineering and Management, Technion, Israel Institute of Technology, Haifa 32000, Israel*

[b] *Department of Electrical Engineering, University of Washington, Seattle, WA 98195, USA*

Received 12 April 1994; revised 28 November 1994

**Abstract**

We treat edge detection as a supervised pattern recognition problem, in which the edge is modeled as a linear combination of basis functions. We show both theoretically and analytically that our selection of Constant, Step and Gaussian as the basis functions is optimal in the sense of minimizing the RMS fitting error. The parameters of these basis functions are learned during the training phase, and the recognition phase uses these learned parameters to locate pixels that belong to edges. This modeling of edges is suitable to edges found in radiographs, which are more complex than step functions. Since edges may appear in any direction, we first show how to determine the gradient direction of the edge. We present the basis functions selected for modeling edges in bone radiographs and show both theoretically and experimentally that they are optimal in the sense that they are the most suitable combination for approximating the bone edge when compared to polynomials with more parameters. We then compute the relevant coefficients and parameters to be used for discriminating between edge and non-edge pixels.

## 1. Introduction

Physical edges of the objects are fundamental descriptions of physical objects as they relate to transitions in surface orientation or texture. Edge detection is the identification of the intensity changes corresponding to the underlying physical changes.

Detecting edges in a radiograph is a first step in taking measurements. Edges in radiographs differ from "conventional" edges, because X-rays, unlike visible light, are only partially absorbed by the object they hit. The physical properties of the object and the width the X-rays must traverse before hitting the photographic film determine the brightness level of each point in the radiograph. Edges in radiographs have therefore a pattern of edge function that is more complex than the step function that models edges in ordinary images. To achieve radiograph understanding, computer systems must relate the raw input data to the physical structure that cause it, i.e., the object being radiated.

Davis (1975) provides a survey of edge detection techniques prior to 1975. One of these methodes is the "gradient" operator $|g(i, j) - g(i+1, j+1)| + |g(i, j+1) - g(i+1, j)|$, proposed by Roberts (Davis,

* Corresponding author. Email: dori@ie.technion.ac.il


*SSDI* 0167-8655(95)00118-9

1975). It detects either a horizontal or a vertical edge, where $g(i, j)$ is the gray-level at point $(i, j)$. Marr and Hildreth (1980) proposed a scheme that has become a standard gauge against which other methods are compared. The basic approach is to convolve the image with a rotationally symmetric Laplacian of Gaussian and to locate zero-crossings of the convolution. A more refined scheme is to declare a pixel to be an edge pixel if it is the zero-crossing of a negatively sloped second directional derivative taken in the direction of the gradient (Haralick, 1984). The Nevatia–Bavu technique (1980) consists of determining the edge magnitude and direction by convolving the image with a number of masks and thinning and thresholding these edge magnitudes. Torre and Poggio (1986) point out that better results may be obtained by using two directional filters with directional derivatives, especially in the neighborhood of corners. Haralick (1984) locates edges at zero-crossings of the second directional derivative in the direction of the gradient. Canny (1983) defines certain desirable criteria for edge detection. He shows that in 1-D the optimal filter is a linear combination of four exponentials, well approximated by a first derivative of a Gaussian. In 2-D images he proposes to use a combination of such filters with varying length, width and orientation. Shen and Castan (1986) propose a linear filter, in which images are convolved with the smoothing function $f(x) = -\frac{1}{2}\ln(b)\, b^{|x|}$ prior to differentiation.

## 2. Edge detection as a supervised pattern recognition problem

Since bone edges in radiographs present a more complicated problem than identifying a step function, we propose a pattern recognition approach to detect these edges. Assuming an edge is perpendicular to the $x$-axis, the intensity of pixels of this edge can be represented analytically as a linear combination of $n$ basis functions as follows:

$$I(x) = \sum_{i=1}^{n} b_i B_i(x, \boldsymbol{P}_i) = (b_1, b_2, b_3, \ldots, b_n) \begin{Bmatrix} B_1(x, \boldsymbol{P}_1) \\ B_2(x, \boldsymbol{P}_2) \\ . \\ \vdots \\ B_n(x, \boldsymbol{P}_n) \end{Bmatrix} = \boldsymbol{bB} \tag{1}$$

Each $B_i(x)$ is a separate basis function evaluated at point $x$ with its coefficient $b_i$ and vector of parameters $\boldsymbol{P}_i = (P_1, P_2, \ldots, P_{j_i})$, where $j_i$ is the number of parameters in the basis function $B_i$ used in the pattern recognition procedure.

Based on this formulation, edge detection is presented as a supervised pattern recognition problem, in which the parameters of the basis functions are learned and calibrated during the learning phase. During the recognition phase, these parameters provide for classifying each pixel as an edge or a non-edge pixel. Fig. 1 represents schematically edge detection as a 2-dimensional pattern recognition decision problem. The training set is used to construct the border between edge and non-edge pixels based on the parameters $b_1$ and $b_2$. In the recognition phase, each pixel is classified as edge or non-edge according to its location in the $b_1$–$b_2$ plane, i.e., its $(b_1, b_2)$ combination using Fisher linear discriminator.

Since edges may appear in any direction, we first develop the mathematical tools to determine the gradient direction of the edge. We then present the selected basis functions for the edge model and show some of their basic characteristics. We show why the selected basis functions are optimal in the sense that when compared to other possibilities of approximating functions, they are the best combination in terms of the number of the involved parameters that need to be approximated. Finally, we devise the scheme for the pattern recognition-based edge detection method.

Fig. 2 depicts the edge model in 3-D, where $(r, c)$ is the image plane (rows and columns of pixels), while the third dimension is the image intensity for each pixel. Either the curve in the wall of the vertebrae or curvature in

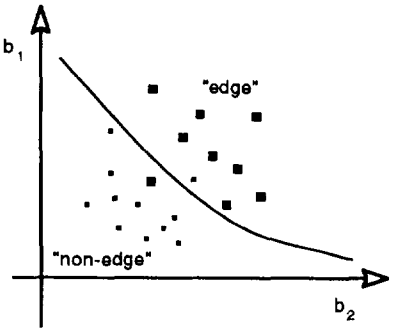


Fig. 1. Discriminating between edge and non-edge pixels in a 2-D parameter space.

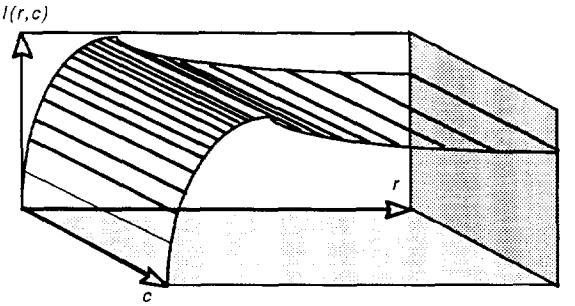


Fig. 2. Radiation intensity through a schematic section of a bone.

the spine may result in an alteration in the orientation, making an angle $\theta$ with the $r$-axis, as shown in Fig. 3. By substituting $x = r\cos\theta + c\sin\theta$ in Eq. (1) we generate a 3-D surface that sweeps the edge curve perpendicular to the gradient direction $\theta$, as shown in Fig. 4 and expressed in Eq. (2), where the parameter vectors $\boldsymbol{P}_i$ are ommitted for brevity.

$$I(r, c) = \sum_{i=1}^{n} b_i B_i(r\cos\theta + c\sin\theta) \tag{2}$$

The partial derivatives of $I$ with respect to $r$ and $c$ are

$$\frac{\partial I(r, c)}{\partial r} = \cos\theta \sum_{i=1}^{n} b_i B_i'(r\cos\theta + c\sin\theta), \qquad \frac{\partial I(r, c)}{\partial c} = \sin\theta \sum_{i=1}^{n} b_i B_i'(r\cos\theta + c\sin\theta).$$

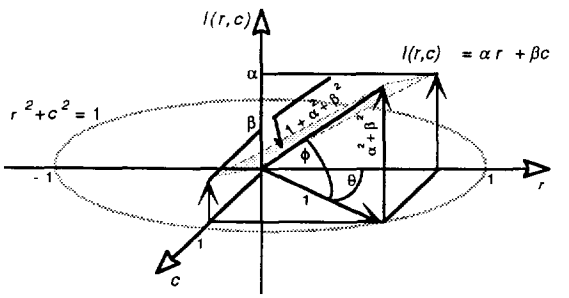


Fig. 3. Inclination angle $\phi$ of the edge intensity plane (the gray parallelogram) and the angle $\theta$ of a unit vector in the gradient direction.

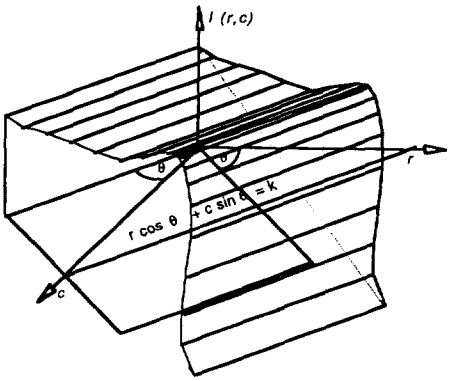


Fig. 4. The intensity of a bone edge making an angle $\theta$ with the $c$-axis.

A unit vector is

$$\vec{g} = \left( \frac{\partial I(r, c)}{\partial r} \quad \frac{\partial I(r, c)}{\partial c} \right)^{\mathrm{T}} \Bigg/ \sqrt{\left( \frac{\partial I(r, c)}{\partial r} \right)^2 + \left( \frac{\partial I(r, c)}{\partial c} \right)^2}$$

$$= \frac{\sum_{i=1}^{n} b_i B_i'(r \cos\theta + c \sin\theta) \begin{pmatrix} \cos\theta \\ \sin\theta \end{pmatrix}}{\sqrt{\left( \sum_{i=1}^{n} b_i B_i'(r \cos\theta + c \sin\theta) \right)^2 (\cos^2\theta + \sin^2\theta)}} = \begin{pmatrix} \cos\theta \\ \sin\theta \end{pmatrix}. \tag{3}$$

To estimate the edge direction, we assume that the neighborhood of a pixel can be approximated as a plane, described in Eq. (4).

$$I(r, c) = \alpha r + \beta c + \gamma + \epsilon(r, c) \tag{4}$$

where $\epsilon(r, c)$ is the error function — the difference between the observed intensity values $I(r, c)$ and the expected ones. To minimize the error in the $(2m + 1) \times (2m + 1)$ neighborhood of the pixel $(r, c)$, we convert Eq. (4) into a least-square problem:

$$\epsilon^2(r, c) = \sum_{r=-m}^{m} \sum_{c=-m}^{m} [I(r, c) - (\alpha r + \beta c + \gamma)]^2 \tag{5}$$

where $(-m, -m)$ and $(m, m)$ are the coordinates of the lower left and upper right corners of the $(2m + 1) \times (2m + 1)$ mask used as an approximation for the plane patch of the pixel under consideration, located at (0, 0). We are looking for $\alpha$, $\beta$ and $\gamma$ which minimize $\epsilon^2$. To find $\alpha$ that minimizes $\epsilon^2$ we take the partial derivative of $\epsilon^2$ with respect to $\alpha$ and equate it to zero:

$$\frac{\partial \epsilon^2}{\partial \alpha} = \sum_{r=-m}^{m} \sum_{c=-m}^{m} 2[I(r, c) - (\alpha r + \beta c + \gamma)](-r) = 0. \tag{6}$$

Opening parentheses, we get:

$$-\sum_{r,c} I(r, c) r + \sum_{r,c} \alpha r^2 + \sum_{r,c} \beta r c + \sum_{r,c} \gamma r = 0 \tag{7}$$

where $\sum_{r,c}$ is shorthand notation for $\sum_{r=-m}^{m} \sum_{c=-m}^{m}$. $\gamma$ is an even function since it is constant. $r$ is an odd function since it is a 45° line passing through the origin. Hence, $\gamma r$ is an odd function and $\sum_{r,c} \gamma r$ is an odd

function taken over limits that are even (i.e., limits that are symmetric around the axes). Since the summation of an odd function taken over such even limits is identically zero, $\sum_{r,c}\gamma r = 0$. Eq. (7) can therefore be written as follows:

$$\sum_{r,c} I(r, c)r = \sum_{r,c} \alpha r^2 + \sum_{r,c} \beta rc. \tag{8}$$

The last term can be written as $\beta(\sum_{r=-m}^{m} r)(\sum_{c=-m}^{m} c)$, where the last two elements are identically zero, yielding

$$\alpha = \left(\sum_{r,c} I(r, c)r\right) / \left(\sum_{r,c} r^2\right) \tag{9}$$

where the denominator is a fixed number $2(2m+1)\sum_{k=1}^{m} k^2$ for a given $m$. For example, if $m = 2$ (a $5 \times 5$ mask), we have:

$$\alpha = \frac{3}{m(m+1)(2m+1)^2} \sum_{r=-m}^{m} \sum_{c=-m}^{m} I(r, c)r = \frac{1}{50} \sum_{r=-2}^{2} \sum_{c=-2}^{2} I(r, c)r. \tag{10}$$

A similar development for $\beta$ yields

$$\beta = \left(\sum_{r,c} I(r, c)c\right) / \left(\sum_{r,c} c^2\right). \tag{11}$$

Since $\gamma$ is the elevation of the plane, it may be taken as zero without loss of generality. To determine the relations between $\alpha$, $\beta$, $r$, and $c$ in the plane $I(r, c) = \alpha r + \beta c + \gamma$, we find $(r, c)$ such that $r^2 + c^2 = 1$ (a unit vector) which maximizes $I(r, c)$. The direction of the vector is the gradient direction. Fig. 3 describes the intensity of the edge gradient making an angle $\theta$ with the $r$-axis.

Using Lagrange multipliers, we get: $e(r, c) = \alpha r + \beta c + \gamma - \lambda(r^2 + c^2 - 1)$. Differentiating, $\partial e/\partial r = \alpha - 2r\lambda = 0 \Rightarrow r = \alpha/2\lambda$, $\partial e/\partial c = \beta - 2c\lambda = 0 \Rightarrow c = \beta/2\lambda$ and $\partial e/\partial\lambda = r^2 + c^2 - 1 = 0$. Substituting $r$ and $c$ in $r^2 + c^2 = 1$, we get $(\alpha/2\lambda)^2 + (\beta/2\lambda)^2 = 1$, which yields $\lambda = \frac{1}{2}\sqrt{\alpha^2 + \beta^2}$, $r = \alpha/\sqrt{\alpha^2 + \beta^2}$, and $c = \beta/\sqrt{\alpha^2 + \beta^2}$. Substituting $r$ and $c$ in the plane $f(r, c) = \alpha r + \beta c + \gamma$ and taking $\gamma = 0$ we get $\alpha^2/\sqrt{\alpha^2 + \beta^2} + \beta^2/\sqrt{\alpha^2 + \beta^2} = \sqrt{\alpha^2 + \beta^2}$, which is the amount we rise by taking a unit step in the gradient direction, as can be seen in Fig. 3. The actual length traversed (see Fig. 3) is $\sqrt{1 + \alpha^2 + \beta^2}$ and the gradient direction is

$$\theta = \tan^{-1}(\alpha/\beta) = \tan^{-1}\left(\left(\sum_{r,c} I(r, c)r\right) / \left(\sum_{r,c} I(r, c)c\right)\right)$$

while the angle of the plane of inclination is

$$\phi = \tan^{-1}\sqrt{\alpha^2 + \beta^2} = \tan^{-1}\sqrt{\left(\sum_{r,c} I(r, c)r\right)^2 + \left(\sum_{r,c} I(r, c)c\right)^2}.$$

Having found $\theta$, the adjustment of our edge model is done by using Eq. (2) rather than Eq. (1).

## 3. The bone model

We model the bone as a hollow pipe whose outer and inner radii are $R$ and $r$, respectively. Fig. 5 shows the length of the path traversed by the X-ray between the two semi-circles denoting the bounds of the outer, hard part of the bone, which blocks most of the radiation.

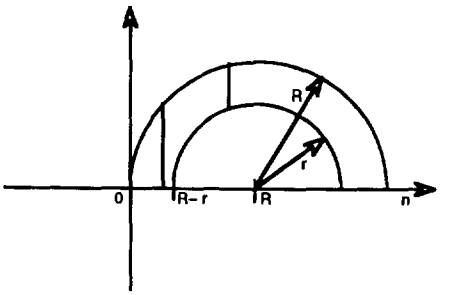


Fig. 5. The length of the outer bone part traveresed by the X-rays.

Define

$$l_n = \begin{cases} \sqrt{\left(R^2 - (R-n)^2\right)} & \text{if } 0 \leqslant n \leqslant R-r, \\ \sqrt{\left(R^2 - (R-n)^2\right)} - \sqrt{r^2 - (R-n)^2} & \text{if } R-r \leqslant n \leqslant R. \end{cases} \tag{12}$$

The optical radiation that remains after passing through a bone of width $l_n$ and hits the X-ray film when the incident radiation is $V_0$ is

$$V_n = V_0(1 - \exp(\alpha l_n)), \tag{13}$$

where $\alpha$ is the absorption coefficient.

For our synthetic experiments, $V_0$ is set such that the root mean square value is always 100:

$$\sqrt{\frac{1}{N}\sum_{n=1}^{N} V_n^2} = 100. \tag{14}$$

Fig. 6 shows the approximate shape of the intensity function of the X-rays that hit the X-ray film.

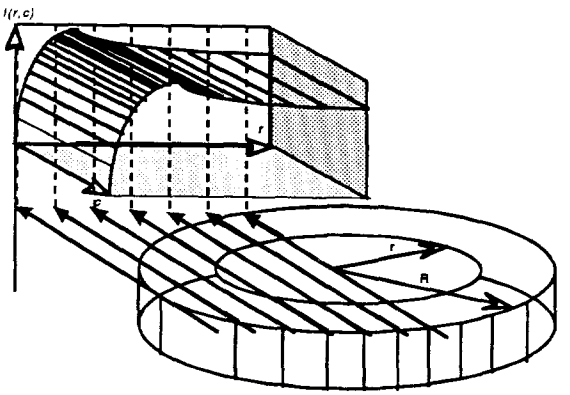


Fig. 6. The approximate shape of the intensity function of the X-rays that hit the X-ray film.

## 4. Basis functions specification

Following Eq. (1), we model the edge of a bone as it appears in a radiograph as a linear combination of three basis functions:

$$V(n) = k_s \text{ Step}(n) + k_g \; g(n) + h_n, \tag{15}$$

where the step function, having slope 1 at its midpoint, is defined by

$$\text{Step}(n) = \begin{cases} -1 & \text{if } 0 \leqslant n < (N-1)/2, \\ 0 & \text{if } n = (N-1)/2, \\ +1 & \text{if } (N-1)/2 < n \leqslant N-1, \end{cases} \tag{16}$$

it models the transition between two tissues with different response to X-ray absorption, where $N$ is odd.

We initially modeled the transition as a hyperbolic tangent, but we found that since the transition is fairly rapid, a simple step function produced essentially the same result without the extra parameter of the hyperbolic tangent.

$g(n)$ is the Gaussian

$$g(n,\sigma) = \exp\left( \frac{1}{2\sigma^2} \left( n - \frac{N+1}{2} \right)^2 \right), \quad n = 0, \ldots, N-1 \tag{17}$$

which models the fact that since the bone is like a hollow pipe, the longest path through the bone is somewhere past the transition point, after which the path length decreases, where $\sigma$ is a parameter that controls the spread of the Gaussian and must be determined from the data.

The determination of the coefficients of the linear combination of the Gaussian and the constant function is just a matter of solving a second-order linear system, once the $\sigma$ of the Gaussian is known. However, when the best $\sigma$ has to be estimated as well, there is additional complexity.

We solved the determination of the best $\sigma$ in the following way. First of all, the determination of $\sigma$ only depends on the even part of the input vector, because the Gaussian is even. For the even part $f$, we first make it monotonically increasing from the first component to the middle component. To do so, we use the idea that the value of the next component of $f$ must be greater than or equal to the previous component.

Let $g$ be the monotone part of $f$, and we set $g_0 = \min\{f_i \mid i = 0, \ldots, N-1\}$. For the next $(N+1)/2 - 1$, i.e., $i = 2, \ldots, (N+1)/2$ components—the left half of the Gaussian—we define $g_i = f_i$ when $f_i > f_{i-1}$ and to be $g_{i-1}$ otherwise. This way we get a vector of size $(N+1)/2$ which approximates the left part of the Gaussian including the middle (top) point.

The last $(N+1)/2 - 1$ components are just the mirror image of the first $(N+1)/2$ components: $g_0 = g_{N-1}$, $g_1 = g_{N-2}$, etc. This way we get a vector $g$ of size $N$: $(g_0, g_1, \ldots, g_{N-1})$.

The next step is to make an initial estimate of the constant coefficient $k$ by which the entire Gaussian is shifted below the horizontal axis. We set this estimate to be $k = 0.001$. We then subtract this constant value from every component of the vector of values $g$—the monotone part of $f$ found earlier—to form the vector $h$. In other words, $h_i = g_i - k \;\; \forall i = 0, 1, \ldots, N-1$.

The method to estimate $\sigma$ is based on the fact that if it were exactly true that

$$h_{n+(N-1)/2} = A \exp(-n^2/2\sigma^2), \tag{18}$$

then

$$\sum_{n=(N-1)/2}^{N} -2 \log[h_{n+1}/h_n] = -1/2\sigma^2[(N-1)/2 - 1]^2. \tag{19}$$

Since $h$ is now known, we calculate

$$a = \sum_{n=(N-1)/2}^{N} -2\log[h_{n+1}/h_n]. \tag{20}$$

$\sigma$ is then extracted and estimated by

$$\sigma = \sqrt{-[(N-1)/2]^2/2a}\,. \tag{21}$$

Having found an estimate for $\sigma$, the components of $h$ are updated by

$$h_n \leftarrow h_n + c\exp\left(-\frac{((N-1)/2)^2}{2\sigma^2}\right) - h_0 \tag{22}$$

where

$$c = \frac{1}{(N-1)/2}\sum_{i=0}^{(N-1)/2} h_{i+(N-1)/2}\exp(-i^2/2\sigma^2). \tag{23}$$

Then we compute a new $a$ and iterate the procedure to get an updated $\sigma$. Convergence of the process is achieved in 10 to 15 iterations.

Since the edge gradient may be in any arbitrary angle $\theta$, we first find $\theta$, then we rotate the coordinate system and interpolate the values sampled in the original coordinate system.

The third basis function, $h(n)$, is the constant unit function, and is described by $h(n) = 1$. Being a constant function, $h(n)$ is obviously even, because $h(-n) = h(n) = 1$. The basis functions Step($n$) and $g(n, \sigma)$ are orthogonal, since we have shown that Step($n$) is odd and $g(n, \sigma)$ is even. Likewise, Step($n$) and $h(n)$ are orthogonal.

Since the basis functions divide as being even or odd, the coefficients for the even basis functions can be solved from a linear system only involving the even basis functions and the coefficient for the one odd basis function can be solved immediately from a one-variable linear equation.

## 5. Justification of the basis function selection

To justify the selection of the three particular basis functions for our problem we performed a set of experiments with both synthetic data based on the bone model and real data taken from a spine radiograph.

The synthetic data was generated using $N = 11$ to 29, and $\alpha$ ranging from 0.05 stepping by 0.05 to 0.5. The bone's outer and inner radii are $R = N/2$ and $r = N/4$, respectively.

We fit the function generated by the bone model to a variety of basis function combinations, including the discrete orthogonal polynomials. The list of those combinations along with the degrees of freedom (number of free parameters) and a representative root mean square residual fitting error for $N = 21$ and $\alpha = 0.025$ is shown in Table 1.

The discrete orthogonal polynomials for a space of dimension $N$ consist of a set of $N$ vectors. The $k$th component of each vector is the value of the polynomial evaluated at the integer $k$. For example, for the vector $V_m = (v_1, \ldots, v_N)$ corresponding to the $m$th order polynomial,

$$v_n = \sum_{i=1}^{N} \alpha_i (n - (N+1)/2)^i. \tag{24}$$

The discrete orthogonal polynomials (DOP) have the property that the even-order polynomials are even functions, and therefore have only even-order terms. Likewise, the odd-order polynomials are odd functions, and

Table 1
RMS performance of various basis functions

| Basis functions | Degrees of freedom | RMS residual | Average RMS per parameter |
|---|---|---|---|
| Order 2 DOP | 3 | 35.07 | 21.64 |
| 1, $G$, $S$ | 4 | 10.60 | 22.35 |
| Order 3 DOP | 4 | 24.23 | 18.94 |
| 1, $S$, $G$, $C$ | 5 | 9.93 | 18.01 |
| 1, $H$, $G$ | 5 | 10.60 | 17.88 |
| Order 4 DOP w/out $Q$ | 5 | 17.64 | 16.47 |
| Order 4 DOP | 5 | 24.16 | 15.17 |
| 1, $H$, $G$, $C$ | 6 | 9.93 | 15.01 |
| Order 5 DOP | 6 | 17.54 | 13.74 |

therefore have only odd-order terms. The coefficients are such that the vectors are orthogonal and have norm one.

The discrete orthogonal polynomials are convenient to use as basis functions since the determination of the coefficients of their linear combination to fit a given vector $x$ is easy. The coefficient for $V_m$ is given by the dot product of $V_m$ and $x$.

Table 1 shows a comparison of a variety of different basis functions. The order of the lines in the table is by degrees of freedom as a first key and within it by RMS residual. The cubic order basis functions we used here for comparison purposes are those used in (Haralick, 1984). The "Average RMS per parameter" column was obtained by subtracting the RMS residual from 100 and dividing the result by the degrees of freedom. Hence, this is a measure of how much, on the average, each parameter (degree of freedom) contributes to the fit.

In terms of average RMS per parameter, the constant-Gaussian-step basis function combination is the best among all the nine combinations in Table 1, scoring 22.35. It is even better than the order 2 DOP, which scored 21.63. Moreover, it is the only one which is not in line with the decreasing order of average RMS per parameter in the table.

The symbol 1 in Table 1 means the constant function taking the value one everywhere. The symbol $G$ means the Gaussian basis function. The symbol $S$ means the step basis function. The symbol $C$ means the discrete orthogonal cubic polynomial. The symbol $Q$ means the discrete orthogonal quartic polynomial. The symbol $H$ means the hypberbolic tangent basis function.

Examining Table 1, it is obvious that the basis functions Constant, Gaussian, Step provide better performance than the cubic polynomial, which is the basis for the zero-crossing of the second directional derivative facet

Table 2
Root mean square fitting errors for the basis functions Constant, Gaussian, and Step for various vector lengths and absorption coefficients

| Row labels: vector length, Column labels: absorption coefficient | 0.050 | 0.100 | 0.150 | 0.200 | 0.250 | 0.300 | 0.350 | 0.400 | 0.450 | 0.500 |
|---|---|---|---|---|---|---|---|---|---|---|
| 11 | 16.58 | 15.52 | 14.68 | 14.04 | 13.59 | 13.28 | 13.11 | 13.03 | 13.02 | 13.06 |
| 13 | 18.52 | 16.90 | 15.58 | 14.57 | 13.84 | 13.35 | 13.06 | 12.92 | 12.90 | 12.95 |
| 15 | 15.87 | 14.41 | 13.33 | 12.60 | 12.17 | 11.98 | 11.95 | 12.05 | 12.21 | 12.40 |
| 17 | 17.34 | 15.29 | 13.74 | 12.66 | 12.00 | 11.69 | 11.61 | 11.69 | 11.86 | 12.06 |
| 19 | 15.26 | 13.37 | 12.04 | 11.23 | 10.85 | 10.78 | 10.90 | 11.13 | 11.40 | 11.68 |
| 21 | 16.45 | 14.00 | 12.24 | 11.14 | 10.60 | 10.47 | 10.58 | 10.82 | 11.10 | 11.38 |
| 23 | 14.81 | 12.52 | 10.97 | 10.12 | 9.82 | 9.88 | 10.13 | 10.46 | 10.79 | 11.10 |
| 25 | 15.76 | 12.96 | 11.04 | 9.96 | 9.57 | 9.61 | 9.87 | 10.21 | 10.55 | 10.86 |
| 27 | 14.45 | 11.79 | 10.06 | 9.22 | 9.03 | 9.22 | 9.57 | 9.96 | 10.32 | 10.63 |
| 29 | 15.11 | 12.03 | 10.00 | 9.01 | 8.79 | 9.00 | 9.37 | 9.77 | 10.14 | 10.45 |

Table 3
Root mean square fitting errors for basis functions consisting of the discrete orthogonal polynomials up through order 3 (cubic) for the same vector lengths and absorption coefficients as in Table 2

| Row labels: vector length, Column labels: absorption coefficient | | | | | | | | | | |
|---|---|---|---|---|---|---|---|---|---|---|
| | 0.050 | 0.100 | 0.150 | 0.200 | 0.250 | 0.300 | 0.350 | 0.400 | 0.450 | 0.500 |
| 11 | 27.16 | 26.60 | 26.14 | 25.77 | 25.49 | 25.27 | 25.10 | 24.98 | 24.88 | 24.82 |
| 13 | 25.73 | 25.16 | 24.76 | 24.49 | 24.33 | 24.25 | 24.22 | 24.24 | 24.29 | 24.35 |
| 15 | 26.48 | 25.83 | 25.37 | 25.06 | 24.86 | 24.75 | 24.70 | 24.70 | 24.72 | 24.76 |
| 17 | 25.77 | 25.07 | 24.63 | 24.38 | 24.29 | 24.28 | 24.34 | 24.44 | 24.55 | 24.66 |
| 19 | 25.99 | 25.29 | 24.85 | 24.62 | 24.53 | 24.53 | 24.59 | 24.68 | 24.78 | 24.88 |
| 21 | 25.59 | 24.82 | 24.40 | 24.24 | 24.23 | 24.32 | 24.46 | 24.62 | 24.77 | 24.92 |
| 23 | 25.63 | 24.89 | 24.51 | 24.37 | 24.38 | 24.49 | 24.63 | 24.79 | 24.94 | 25.08 |
| 25 | 25.38 | 24.58 | 24.22 | 24.15 | 24.24 | 24.41 | 24.61 | 24.81 | 25.00 | 25.16 |
| 27 | 25.34 | 24.59 | 24.28 | 24.24 | 24.36 | 24.55 | 24.75 | 24.95 | 25.13 | 25.28 |
| 29 | 25.18 | 24.37 | 24.09 | 24.12 | 24.30 | 24.54 | 24.79 | 25.01 | 25.21 | 25.37 |

edge operator (Haralick, 1984). No significant difference has been found between the step and the hyperbolic tangent, and since the step involves only one parameter, as opposed to two for the hyperbolic tangent, its average RMS per parameter is better: 22.35 vs. 17.88.

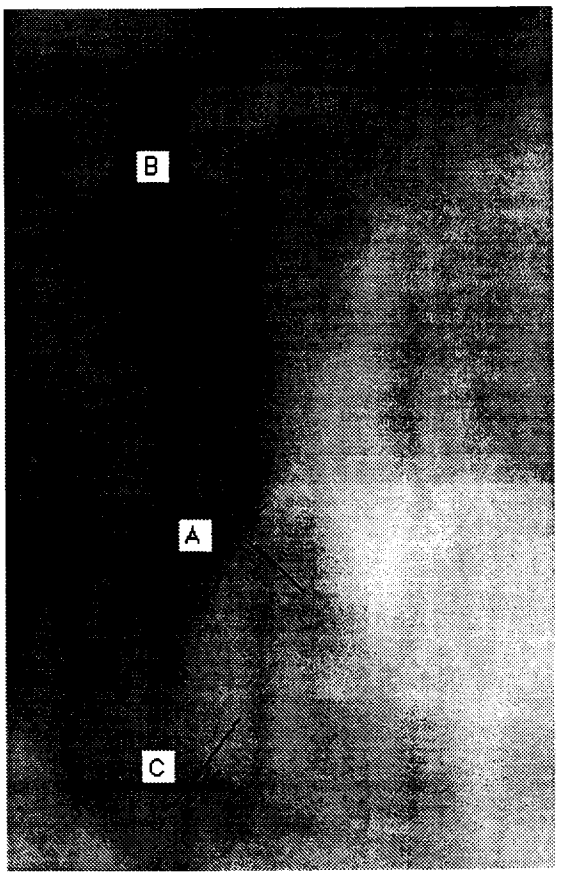


Fig. 7. The three edge cross-sections marked A, B and C sampled from the vertebrae radiograph.

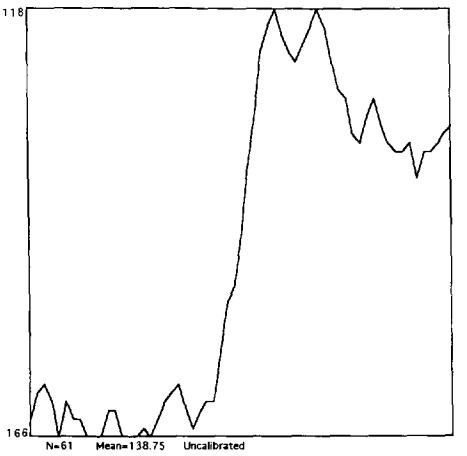


Fig. 8. The graph of cross-section A in Fig. 7.

Table 2 shows the root mean square errors for fitting the basis functions Constant, Gaussian, and Step to the bone model for various vector lengths and absorption coefficients. Table 3 shows the same root mean square fitting errors for the set of basis functions consisting of the discrete orthogonal polynomials up through order 3 (cubic) for the same vector lengths and absorption coefficients as in Table 2.

Looking at the two tables we can see that changing either the absorption coefficient or the vector length has only a very limited effect on the RMS error. A comparison of the two tables shows, however, that our basis function combination of Constant, Gaussian, and Step, which has 4 degrees of freedom, has an RMS error which is smaller by about 80% than that of the basis function set consisting of the discrete orthogonal polynomials up through order 3 (cubic), which have the same number (4) of degrees of freedom.

The real data, which was taken from a spine vertebrae, was sampled from a line drawn on a digitized radigraph, as shown in Fig. 7. It shows the three edge cross-sections marked A, B and C sampled from the vertebrae radiograph.

Figs. 8, 9 and 10 show the three graphs resulting from cross-sections A, B and C of Fig. 7, respectively.

The lengths in pixel units of the three cross-sections are 61, 41 and 47. Each cross-section was sampled to have 15 components. Examining the results of Table 4, we can see that in all three cases A, B and C, the "1, $G$,


Fig. 9. The graph of cross-section B in Fig. 7.


Fig. 10. The graph of cross-section C in Fig. 7.

Table 4
RMS performance of the various basis functions on the three cross-sections marked A, B and C in Fig. 7

| Basis functions | Degrees of freedom | A RMS residual | B RMS residual | C RMS residual |
|---|---|---|---|---|
| Order 2 DOP | 3 | 9.97 | 7.13 | 4.28 |
| 1, $G$, $S$ | 4 | 4.37 | 2.63 | 1.64 |
| Order 3 DOP | 4 | 6.31 | 5.37 | 2.70 |
| 1, $S$, $G$, $C$ | 5 | 3.95 | 2.53 | 1.64 |
| 1, $H$, $G$ | 5 | 4.37 | 2.63 | 1.63 |
| Order 5 DOP w/out $Q$ | 5 | 4.70 | 4.50 | 2.26 |
| Order 4 DOP | 5 | 6.21 | 4.75 | 2.68 |
| 1, $H$, $G$, $C$ | 6 | 3.95 | 2.53 | 1.64 |
| Order 5 DOP | 6 | 4.56 | 3.74 | 2.24 |

$S$'' (Constant, Gaussian, Step) basis function combination has the best performance among the basis functions with 4 parameters and is almost as good as the best among the ones with 5 coefficients. In particular, it yields the same results as the ''1, $G$, $H$'', where the step is replaced by a hyperbolic tangent, hence adding an extra degree of freedom. It even performs better than an order 5 DOP with 6 degrees of freedom.

## 6. Summary and future work

We have discussed a notion of edge that is more general than a mere step function and suits the description of edges in radiographs. The pattern-based edge detection starts with supervised learning, in which the user teaches the system what are the pixels in the displayed radiograph that should be considered as edges by pointing at those pixels. The system analyses the selected image points and computes the values of the five parameters $\theta$, $\sigma$, $k_f$, $k_g$, $k_h$ according to the process described. We have shown both theoretically and analytically that our selection of Constant, Step and Gaussian as the basis functions is optimal in the sense of minimizing the RMS fitting error.

The edge pixel sample size is determined by the variation of the values formed for each parameter. Having found the values of $\theta$, $\sigma$, $k_f$, $k_g$, $k_h$, we devise a method to answer the question: Given a pixel $(r, c)$ in the input image, does it belong to an edge or not?

The proposed procedure is as follows. (1) Find the six-dimensional classification function for any input pixel $(r, c)$, which classifies the pixel as "edge" or "non-edge". (2) Classify each pixel in the image as "edge" or "non-edge" according to the classification function.

Work must be done in order to adapt the discrimination function that fits the problem at hand. Human-machine interface for efficient learning should also be devised. Finally, the effectiveness of the method should be tested in practice. The detected edge points may serve a number of functions. First, they may as anchors for traditional orthopaedic measurements. The angle of curvature of the spine is one such measurement. Alternately, objective measurements such as cortical area of implants may made where previously subjective interpretation was thought to be adequate. In both cases, great precision is brought to bear upon the decision process. The numbers obtained from the computer radiograph may be at odds with those determined by the physician by hand. Hence, inter-observer variation will still exist. However, the issue of intra-observer variation is essentially eliminated.

## References

Canny, J.F. (1983). Finding edge and lines in images. MIT Artificial Intelligence Lab. Tech. Report 720, June 1983.

Davis, L.S. (1975). Survey of edge detection techniques. *Computer Graphics and Image Processing* 4, 248–270.

Haralick R.M. (1984). Zero-crossing of second directional derivative edge operator. *IEEE Trans. Pattern Anal. Machine Intell.* 6 (1), 58–68.

Marr, D. and H. Hildreth (1980). Theory of edge detection. *Proc. Roy. Soc. London* B207, 187–217.

Nevatia, R. and K.R. Bavu (1980). Linear feature extraction and description. *Computer Graphics and Image Processing* 13, 257–269.

Shen, J. and S. Castan (1986). An optimal linear operator for edge detection. *Proc. CVPR-86*, Miami Beach, FL, 109–114.

Torre, V. and T. Poggio (1986). On edge detection. *IEEE Trans. Pattern Anal. Machine Intell.* 8, 147–163.